

The Enigma of Li-Rich Giants and its Relation with Temporal Variations Observed in Radial Velocity and Stellar Activity Signals

Inês Rolo^{1,2}, Elisa Delgado Mena¹, Maria Tsantaki³, João Gomes da Silva¹

¹ Instituto de Astrofísica e Ciências do Espaço, Universidade do Porto, CAUP, Rua das Estrelas, 4150-762 Porto, Portugal

² Departamento de Física e Astronomia, Faculdade de Ciências, Universidade do Porto, Rua do Campo Alegre 687, 4169-007 Porto, Portugal

³ INAF – Osservatorio Astrofisico di Arcetri, Largo E. Fermi 5, 50125 Firenze, Italy

Received Date / Accepted Date

ABSTRACT

Context. Despite the large number of studies focused on the characterization of Li-rich stars and understanding of the mechanisms leading to such enrichment, their origin remains a mystery.

Aims. Magnetic activity, in particular the phenomena usually associated with it, such as spots and plages, and the Li abundance (A(Li)) of stars, are in general thought to be connected. However, as of today it is unclear just how. In this work, we study a sample of young but evolved intermediate mass red giants, inhabitants of open clusters where planets have been searched. We aim at using radial velocity (RV) and stellar activity indicator signals to look for relations between Li abundances and stellar activity/variability.

Methods. We explore how the standard deviation (STD), peak to peak amplitude (PTP), mean and median of typical stellar activity indicators (BIS, FWHM, T_{eff} , and $H\alpha$ index) change as a function of the Li content of 82 red giants. Furthermore, we compute weighted Pearson Correlation Coefficients (ρ_w) between time series of RV measurements and the stellar activity indicators for the stars in our sample. To aid our results, we also study Generalized Lomb-Scargle Periodograms (GLSP) to capture possible significant periodic temporal variations in our data.

Results. Our analysis indicates that the STD and PTP of BIS and FWHM, the mean and median of the $H\alpha$ index and $v \sin(i)$ increase exponentially with A(Li) in our sample of red giants. Significant temporal variations and correlations between RVs and activity indicators also tend to be found preferentially for stars where high A(Li) is observed. Most of the Li-rich stars in our sample either show strong correlations of RV with at least one of the stellar activity indicators or reveal significant periodic temporal variations in their stellar activity indicators GLSPs consistent with those found for RV.

Key words. red-giants – open clusters – lithium rich – stellar activity

1. Introduction

Low ($\lesssim 2M_{\odot}$) to intermediate mass stars ($\sim 2 - 8M_{\odot}$) (Iben 1967a,b), before entering the red giant branch (RGB) of their evolution, go through a mixing episode called the first dredge up (FDU), which destroys most, if not all, of their surface lithium (Li). Stars as massive as the Sun, according to standard stellar evolution models, should not exhibit a surface lithium abundance, A(Li)¹, exceeding 1.5 dex after the FDU. In general, observations concur this but $\sim 1\%$ of observed giants (e.g. Brown et al. 1989; Kumar et al. 2011; Liu et al. 2014; Casey et al. 2016; Kirby et al. 2016; Deepak & Reddy 2019; Gao et al. 2019; Pabst et al. 2020; Martell et al. 2021) present abnormally high A(Li) with the highest abundance observed to date in a red giant star being 5.62 dex (Kowkabany et al. 2022). These stars are known as Li-rich giants.

Possible explanations for the Li enrichment observed in these stars fall under two main categories. First, it has been proposed that a star may show high levels of surface Li if it has been contaminated by an external source. For example, if planet engulfment occurs, the Li content of the planet can be laid out in the photosphere of the star and enrich it (e.g. Adamów et al. 2012; Aguilera-Gómez et al. 2016; Delgado Mena et al. 2016). On the other hand, under certain conditions Li can be synthe-

sized inside a star and rise to the surface through extra mixing processes. For stars with mass $> 4M_{\odot}$ in the asymptotic giant branch (AGB) of their evolution, the Cameron-Fowler Mechanism (CFM) (Cameron & Fowler 1971) is the preferred scenario to explain Li enrichment. In these stars the temperature at the bottom of the convective envelope is favourable to the production of beryllium which, when transported to the outer layers of the star fast enough, can produce Li without it being destroyed. In lower mass stars, high enough temperatures for beryllium production can only be found inwards of the convective envelope. For these stars the existence of extra mixing mechanisms such as thermohaline mixing (e.g. Eggleton et al. 2008; Cantiello & Langer 2010) and rotation induced mixing (e.g. Denissenkov & Herwig 2004; Palacios et al. 2004; Adamów et al. 2014) are more plausible as they are needed to bring the beryllium from the deeper layers to the convective envelope so that CFM can ensue. One way to probe extra mixing scenarios is by analysing the surface carbon isotopic ratio $^{12}\text{C}/^{13}\text{C}$, which after the FDU is lowered to values of about 20-30 (Charbonnel 1994; Denissenkov & Herwig 2004). Further lowering of $^{12}\text{C}/^{13}\text{C}$ is a good, and widely used, indicative that extra mixing occurred in a star (Charbonnel 1995; Aguilera-Gómez et al. 2023; Lagarde et al. 2024).

It is also generally accepted that higher than normal A(Li) is common among magnetically active stars, even if the reason for

¹ $A(\text{Li}) = \log[N(\text{Li})/N(\text{H})] + 12$

this is still poorly understood. This has been evidenced for different types of stars namely dwarfs (Favata et al. 1996; Zboril et al. 1997), magnetically peculiar stars (see Lyubimkov 2016 for a review), active binaries and pre-main-sequence stars (Pallavicini et al. 1992), active main sequence and zero-age main sequence stars (Xing et al. 2021) and active giant stars (Fekel & Balachandran 1994; Sneden et al. 2022).

In this work, we are interested in studying the possible connection between Li enhancement in red giant stars and their stellar activity. For this we start by looking for relations between several descriptive statistics of stellar activity indicators and A(Li) in a sample of red giant stars, some of which are lithium rich, where planets have been searched. These stars are inhabitants of open clusters, which is particularly favourable, as we are able to better constrain their evolutionary status. To strengthen our analysis we also look for correlations as well as periodic temporal variations in stellar activity signals that may connect variability observed in radial velocity (RV) to stellar activity. The present article is organized as follows, in Sect. 2 we provide an overview of our data. In Sect. 3 we explain the methods incurred in the data analysis. In Sect. 4 we discuss our results, and the main conclusions are laid out in Sect. 5.

2. Observations and Sample

Our sample is comprised of young but evolved intermediate mass red giants resident in 10 different open clusters (IC4651, IC4756, NGC2345, NGC2423, NGC3114, NGC3532, NGC3680, NGC4349, NGC5822 and NGC6705). These stars have been observed over the years with the HARPS spectrograph (Mayor et al. 2003) at the ESO 3.6-metre telescope (R=115 000) and the CORALIE spectrograph (Queloz et al. 2000; Udry et al. 2000) at the Swiss 1.2-metre Leonhard Euler Telescope at ESO’s La Silla Observatory (R=60 000), as part of a program to search for exoplanets. For a complete description of the RV surveys see Lovis & Mayor (2007); Delgado Mena et al. (2018); Delgado Mena et al. (2023). The stellar parameters and Li abundances for this sample are presented in Tsantaki et al. (2023), obtained using the same spectra employed here.

In this work, the data available from CORALIE will not be treated. CORALIE data carries a much higher associated uncertainty in the measurements than HARPS data, due to its significantly lower resolution (R). Furthermore, CORALIE data was only collected for a subset of the stars in our sample, and the measurements for each star are few in number. For these reasons it is preferable to use only HARPS data.

Only stars with 5 or more observational data points were considered for analysis. This is such to increase the credibility of our results, while including the highest amount of observed stars possible. In total, 82 stars were analysed out of which 15 are canonically Li-rich, that is, show $A(\text{Li}) > 1.5$ dex. If a Population I star forming with a metallicity alike that of the Sun has in the beginning of its life $A(\text{Li}) \sim 3.3$ dex, that is, the approximate A(Li) of the interstellar medium, accounting for the dilution occurring during the FDU, in the red giant phase of its evolution it should be left with a maximum of $A(\text{Li}) \sim 1.5$ dex (e.g. Charbonnel & Balachandran 2000). Studying stars in open clusters, however, allows for a more precise estimate of this limit. Open clusters are ideal laboratories for studying Li enhancement given that they provide natural constraints on mass, composition, age and evolutionary state of their members. With such information it is possible to estimate the amount of Li that all stars in a given cluster should have at their current age using stellar evolution models. This allows us to better constrain what makes a star in

a given cluster “Li-rich” (see Sun et al. 2022). Tsantaki et al. (2023) conducted such a study, providing estimations for the maximum A(Li) that stars in 32 different open clusters should have in their current evolutionary stage. Stars will be considered Li-rich according to the limits defined in Table 1 and the canonical definition. Special attention will also be given to stars that show high Li content in comparison with inhabitants of the same cluster in the same evolutionary stage, these will be deemed ‘Li-Rich-in-Context’ in accordance with Tsantaki et al. (2023) and Sun et al. (2022). All relevant stars come presented in Table 2. Some of these stars have been previously studied in the literature. A thorough discussion concerning the possible nature of the Li enrichment observed in these stars has been provided in Tsantaki et al. (2023), and is summarized in Table 2.

Cluster	A(Li) _{max} [dex]	[Fe/H] [dex]
IC4651	1.46	-0.01
IC4756	1.26	-0.12
NGC2345	1.37	-0.22
NGC2423	1.46	-0.03
NGC3114	1.46	-0.10
NGC3532	1.40	-0.08
NGC3680	1.26	-0.15
NGC4349	1.26	-0.11
NGC5822	1.46	-0.10
NGC6705	1.54 ⁽¹⁾	0.07

Table 1: Limits over which a star can be considered lithium rich according to Tsantaki et al. (2023) for every cluster in our sample ($A(\text{Li})_{\text{max}}$ [dex]), as well as the metallicity of each cluster ([Fe/H]). (1) As derived in Randich et al. (2020); Romano et al. (2021).

3. Methods

To probe if the high A(Li) that we observe in red giant stars is connected to their stellar activity we explore two methods. First, we study how Li abundances relate to these five stellar activity indicators:

1. the bisector inverse slope (BIS) of the cross correlation function;
2. the full width at half maximum (FWHM) of the cross correlation function;
3. the H_{α} index with both a 0.6 Å and 1.6 Å central bandpass ($H_{\alpha}06$, $H_{\alpha}16$);
4. and the effective temperature (T_{eff}).

In particular, we look for relations between A(Li) and the standard deviation (STD) and peak to peak amplitude (PTP) of all stellar activity indicators as well as the mean and median of H_{α} . Only statistically significant models at a 99% confidence level (with p-values of the F-test < 0.01) will be discussed.

Secondly, we would like to investigate if a possible connection between A(Li) and stellar activity is manifested in RV variability. So, we seek correlations between stellar activity indicators and RV measurements (see Figure A.1). These will be computed according to the Pearson Correlation Coefficient, ρ_w , which is here weighted by the uncertainty in the measurements. P-values for each correlation will also be provided to attest the statistical significance of the correlations. A p-value below 0.05 suggests that the correlation is significantly different from 0 at a

Star	A(Li) _{NLTE} [dex]	Li-Rich Type	Evolutionary Stage	Mass [M _⊙]	$v \sin(i)$ [km/s]	¹² C/ ¹³ C	Possible Li Production Mechanism
IC4651No6333	1.21	In Context	luminosity bump	1.78	2.13	-	Extra-Mixing
IC4651No9791	1.28	In Context	luminosity bump	1.75	1.85	-	Extra-Mixing
IC4756No52 (*)	1.45	>A(Li) _{max}	RGB tip	2.27	2.87	-	Unknown
NGC2345No50	0.98	In Context	RGB/early AGB	5.84	5.27	(>)26 ^(ξ)	Unknown/HBB
NGC2423No3	1.38	In Context	RGB-Lum. bump?	2.04	2.19	-	Unknown
NGC3114No170 ^(#)	1.50	Canonical	red clump	3.98	11.32	(≥) 24 ^(##)	Planet Accretion/Tidal Interactions
NGC3532No19	1.44	>A(Li) _{max}	red clump	3.22	5.05	12 ^(†)	Extra-Mixing ^(δ)
NGC3532No649 ^(b)	3.27	Canonical	-	2.17	-	10 ^(‡)	Extra-Mixing
NGC3532No670	1.47	>A(Li) _{max}	RGB tip	3.05	4.64	20 ^(†)	Unknown
NGC3680No13	1.25	In Context	luminosity bump	1.66	0.28	16 ^(ζ)	Extra-Mixing
NGC3680No53	1.21	In Context	luminosity bump	1.65	0.12	10 ^(ζ)	Extra-Mixing
NGC4349No9	1.26	=A(Li) _{max}	red clump	3.00	9.58	16 ^(*)	Planet Accretion/Tidal Interactions
NGC4349No127	1.37	>A(Li) _{max}	RGB tip	3.01	4.81	18 ^(*)	Unknown
NGC5822No102	1.34	In Context	RGB base/red clump	2.02	5.83	-	Unknown
NGC5822No240	1.40	In Context	RGB tip	2.07	2.83	17 ^(†)	Extra-Mixing
NGC6705No1101	1.53	Canonical	RGB base	3.67	11.24	-	Li-rich Formation Environment
NGC6705No1117	1.57	Canonical	red clump	3.52	9.44	-	Li-rich Formation Environment
NGC6705No1248	1.52	Canonical	red clump	3.46	8.43	-	Li-rich Formation Environment
NGC6705No1256	1.59	Canonical	RGB	3.15	4.47	-	Li-rich Formation Environment
NGC6705No1364	1.53	Canonical	red clump	3.67	12.24	-	Li-rich Formation Environment
NGC6705No1658	1.51	Canonical	red clump	3.91	7.29	-	Li-rich Formation Environment
NGC6705No411	1.57	Canonical	RGB	3.19	6.47	-	Li-rich Formation Environment
NGC6705No660	1.53	Canonical	red clump	3.58	5.74	-	Li-rich Formation Environment
NGC6705No669	1.51	Canonical	red clump	3.45	8.93	-	Li-rich Formation Environment
NGC6705No779	1.57	Canonical	RGB	3.40	5.57	-	Li-rich Formation Environment
NGC6705No816	1.53	Canonical	red clump	3.96	8.77	-	Li-rich Formation Environment
NGC6705No916	1.53	Canonical	red clump	3.75	9.70	-	Li-rich Formation Environment
NGC6705No963	1.54	Canonical	red clump	3.76	6.71	-	Li-rich Formation Environment

Table 2: Li-rich (canonical and above the A(Li) limits listed in Table 1, >A(Li)_{max}) and ‘Li-Rich-in-Context’ giants present in our sample. Stellar parameters are as derived in Tsantaki et al. (2023) or otherwise specifically stated.

Notes: (δ) This work; (#) Possible non-member: Katime Santrich et al. (2013). (##) As derived in Katime Santrich et al. (2013). (†) As derived in Smiljanic, R. et al. (2009). (‡) As derived in Luck (1994). (b) Non-member: Mermilliod et al. (2008). (●) Possible non-member: Herzog et al. (1975); Frinchaboy & Majewski (2008); Bagdonas et al. (2018). (*) As derived in Holanda et al. (2022). (ξ) As derived in Holanda et al. (2019). (ζ) As derived in Peña Suárez et al. (2018).

95% confidence level. In addition, periodic temporal variations of the RV measurements of these stars and the stellar activity indicators will be analysed by drawing Generalized Lomb-Scargle Periodograms (GLSP) (Zechmeister & Kürster 2009), to evaluate if they connect to the presence of Li.

When searching for planets it is important to devise methods to distinguish planetary signals from temporal variability that may arise from the phenomena appearing at the surface of the star as a consequence of stellar magnetic activity. The BIS and FWHM values of each observation are provided by the HARPS data reduction pipeline as part of the process to calculate the RV of a given spectrum. Correlations found between RV and respective BIS and FWHM measurements indicate that periodical variability noticed in RV signals may originate from stellar activity or stellar surface inhomogeneities, rather than planets. Variability observed in BIS and FWHM over time with approximately the same period as that observed in RV, can also further corroborate this. These types of studies have often been conducted to probe whether or not a planet really exists in orbit of a certain star (e.g. Queloz et al. 2001; Delgado Mena et al. 2018).

In studying how stellar activity impacts an RV signal, it is common to analyse spectral lines that serve as an activity proxy due to their well known correlations with the existence of active regions in the surface of the star. One such spectral line is the H_α line. Here, we determine H_α index values from spectra using

ACTIN 2² (Gomes da Silva et al. 2018, 2021). This tool to calculate stellar activity indices provides two measurements for the H_α index for two different central bandpasses: 0.6 Å and 1.6 Å (see Figure A.2). Since it has been mostly used for dwarf stars (Gomes da Silva et al. 2022), there is a lack of an extensive study for stars as the ones in our sample, and it is not clear which central bandpass is optimal for the study of these stars. Recently, in analysing the strong RV signals of some of the stars in this sample (Delgado Mena et al. 2023), we found that H_α16 seems to be a more reliable activity indicator for these evolved stars. But this conclusion was based on a small sample. As such, and since the two bandpasses probe the stellar atmosphere at different layers being sensitive to different phenomena, in our analysis both are used.

We further extend our search for correlations and periodical variations to the T_{eff}. Manifestations of magnetic activity, much like spots and plagues are usually accompanied by temperature variations. Spots are cooler than their surrounding photosphere, while plagues are hotter than their surrounding chromosphere. During periods of intense magnetic activity it is possible that, if the T_{eff} is affected, the variations observed could correlate with the activity induced variations (e.g. Yana Galarza et al. 2019). We use the stellar spectral analysis package, FASMA³ (Tsantaki et al. 2018), to determine the T_{eff} from individual stellar spectra.

² <https://github.com/gomesdasilva/ACTIN2>

³ <https://github.com/MariaTsantaki/FASMA-synthesis>

FASMA relies on the radiative transfer code MOOG⁴ (Snedden 1973) to model the atmosphere and create a synthetic spectrum for a set of input parameters (surface gravity, $\log(g)$; iron metallicity, $[\text{Fe}/\text{H}]$; macro-turbulence velocity v_{mac} ; and projected rotational velocity $v \sin(i)$) of a given star. The synthetic spectrum is then statistically compared to the observed spectrum of the star and the parameters are iteratively adjusted using a non-linear least-squares algorithm to find the set that best fits observations. To capture reliable variations in T_{eff} , when computing it, we fix all other input stellar parameters, and leave T_{eff} to be computed freely for each individual stellar spectra. Stellar parameters for the stars in our sample have been derived in Tsantaki et al. (2023) also using FASMA.

4. Results and Discussion

As presented in Table 2 and in accordance with Mermilliod et al. (2008), the star NGC3532No649 is not a member of cluster NGC3532 making the calculation of its mass and evolutionary stage uncertain. For this reason, it will not be included in the following discussion despite it being Li-rich.

4.1. Is the Lithium Abundance of Red Giants related to Stellar Activity?

We start by analysing the dispersion (STD and PTP) of BIS, FWHM, T_{eff} and $H\alpha$ to probe potential connections between activity variability and $A(\text{Li})$. We also test if the mean and median of $H\alpha$, indicative of a star's activity level, is related to $A(\text{Li})$. For the computation of these relations we only use stars with $A(\text{Li}) > -0.5$ as this is the limit of FASMA's minimization algorithm in the determination of $A(\text{Li})$ (Tsantaki et al. 2023). Using these limit values would be a source of bias. We find that the STD and PTP of BIS and FWHM increase exponentially with $A(\text{Li})$ and the mean and median values of $H\alpha 06$ also increase exponentially with $A(\text{Li})$. In particular, the vast majority of stars with high $H\alpha 06$ index are Li enriched. On the other hand, we do not find $A(\text{Li})$ to be related to $H\alpha 16$. These results suggest that the activity levels of the stars in our sample seem to increase with increasing $A(\text{Li})$. These results are in agreement with Sneden et al. (2022) who found that Li-rich giants are more chromospherically active when in comparison to their Li poor counterparts, as they are more likely to show strong He I10830 absorptions. We also find that $v \sin(i)$ correlates well with dispersion of BIS and FWHM as well as the mean and median of the $H\alpha 06$ index. This is indicative that more magnetically active stars also tend to rotate faster. Gonçalves et al. (2020) also arrived at a similar conclusion. The best fit relations are listed in Table 3. Plots of the relations found for STD of BIS and FWHM as well as the mean of $H\alpha 06$ are shown in Figure 1. The plots for PTP of BIS and FWHM and the median of $H\alpha 06$ look similar to the ones shown in Figure 1 and are presented in Appendix B. Also in Appendix B are plots of the mean and median $H\alpha 16$ as a function of $A(\text{Li})$, for which no clear relation was found. In addition to the results of the F-test, in Table 3 we also provide R^2 values, with better fits having R^2 closer to 1. R^2 values for the relations we find are in general low as there is significant scatter around the lines of best fit.

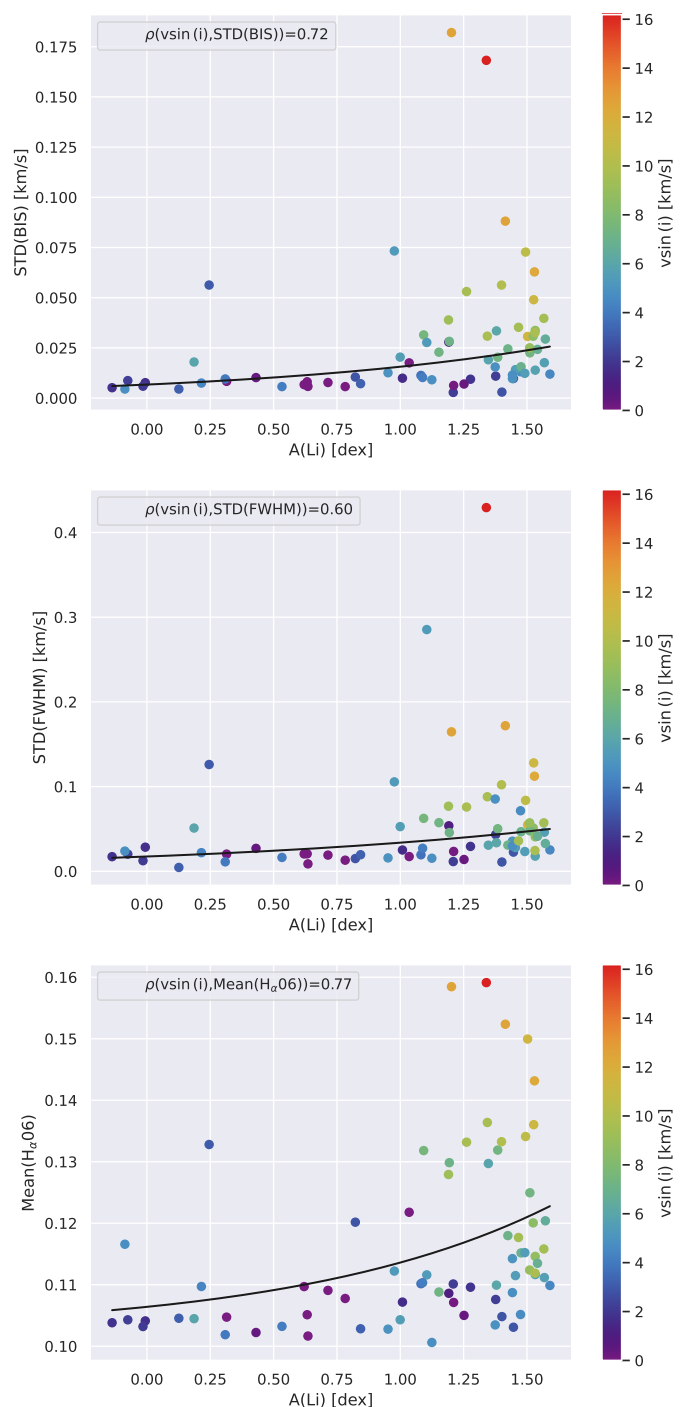


Fig. 1: Exponential relation found between the STD of BIS data for each star and $A(\text{Li})$ [top panel]; the STD of FWHM data for each star and $A(\text{Li})$ [middle panel]; the mean of $H\alpha 06$ data for each star and $A(\text{Li})$ [bottom panel]. The data points are colored according to the $v \sin(i)$ of each star. The black lines are the lines of best fit for which the F-test statistics and p-values are listed in Table 3. In these plots we also show the Pearson Correlation Coefficients (ρ) between the activity proxies used and $v \sin(i)$, all of them being very strong (> 0.6).

Formula	F-Statistic	p(F-Statistic)	R ²
STD(BIS)=0.0067e ^{0.84A(Li)}	20.62	2.2×10 ⁻⁵	0.22
STD(FWHM)=0.017e ^{0.66A(Li)}	13.59	0.0004	0.16
PTP(BIS)=0.024e ^{0.84A(Li)}	18.66	4.93×10 ⁻⁵	0.21
PTP(FWHM)=0.060e ^{0.66A(Li)}	11.73	0.001	0.14
Mean _{Hα06} =0.004e ^{A(Li)} + 0.1	11.55	0.001	0.14
Median _{Hα06} =0.004e ^{A(Li)} + 0.1	12.12	0.0009	0.14
v sin(i)=1.69e ^{A(Li)} - 0.2	34.82	1.09×10 ⁻⁷	0.33

Table 3: Best fit relations of the descriptive statistics of the stellar activity indicators and $v \sin(i)$ as a function of $A(\text{Li})$. These are accompanied by the respective F-Statistic for each relation and its p-value, as well as R².

4.2. Manifestation of Stellar Activity in RV signals and its Connection to Lithium Enhancement

To further investigate these findings, we also looked at how RV variability correlates with the stellar activity indicators and whether this is linked to $A(\text{Li})$. All the correlations discussed here are shown in Figure 2 and listed in Appendix C. From our analysis, 22/81 stars show a strong correlation ($>0.4^5$) between the RV variability and the BIS variability. The majority of the correlations were found to be negative. We noticed that 13/22 of the strong correlations found between RV and BIS appear for stars that are moderate and fast rotators, that is, show $v \sin(i) > 5 \text{ km/s}$ (e.g. de Medeiros et al. 1996; Tayar et al. 2015; Patton et al. 2023). This is likely a consequence of this diagnostic of line asymmetry losing sensitivity for slower rotators (e.g. Santos et al. 2003). There is, however, evidence in the literature (e.g. Carlberg et al. 2012; Sneden et al. 2022; Sayeed et al. 2023; Tsantaki et al. 2023) that there is a connection between Li enrichment in giants and $v \sin(i)$. This is also suggested in our sample as we find that $v \sin(i)$ increases exponentially with $A(\text{Li})$ (shown in Appendix B and Table 3). Out of the 27 Li-rich stars listed in Table 2, 8 stars show strong correlations between RV and BIS.

In what concerns the FWHM, 20/81 stars show strong correlations with RV measurements. The correlations are preferentially positive. 6 of the Li-rich stars in our sample show strong correlations between RV and FWHM.

For the T_{eff} we find that 15/81 stars show strong correlations with RV measurements. Correlations between the RV and T_{eff} are mostly positive. Only 3 of the Li-rich stars show strong correlations between RV and T_{eff} . There is a possibility that this is such because the individual spectra used to measure T_{eff} values to look for variations may not have a signal to noise ratio high enough for this purpose.

As for $H\alpha 16$, 20/81 stars show strong correlations with RV, which are mostly negative. 9 of the Li-rich stars show strong correlations between RV and $H\alpha 16$.

Last but not least for $H\alpha 06$, 19/81 stars show significant correlations with RV measurements, which are preferentially positive. We find that 10 of the Li-rich stars in our sample show strong correlations between RV and $H\alpha 06$.

⁴ <https://www.as.utexas.edu/~chris/moog.html>

⁵ Some of the analysed stars in our sample do not have a large number of data points. Because of this we chose to include moderate correlations which have the potential to become strong with the addition of new data. For ease of nomenclature we refer to all correlations >0.4 as strong.

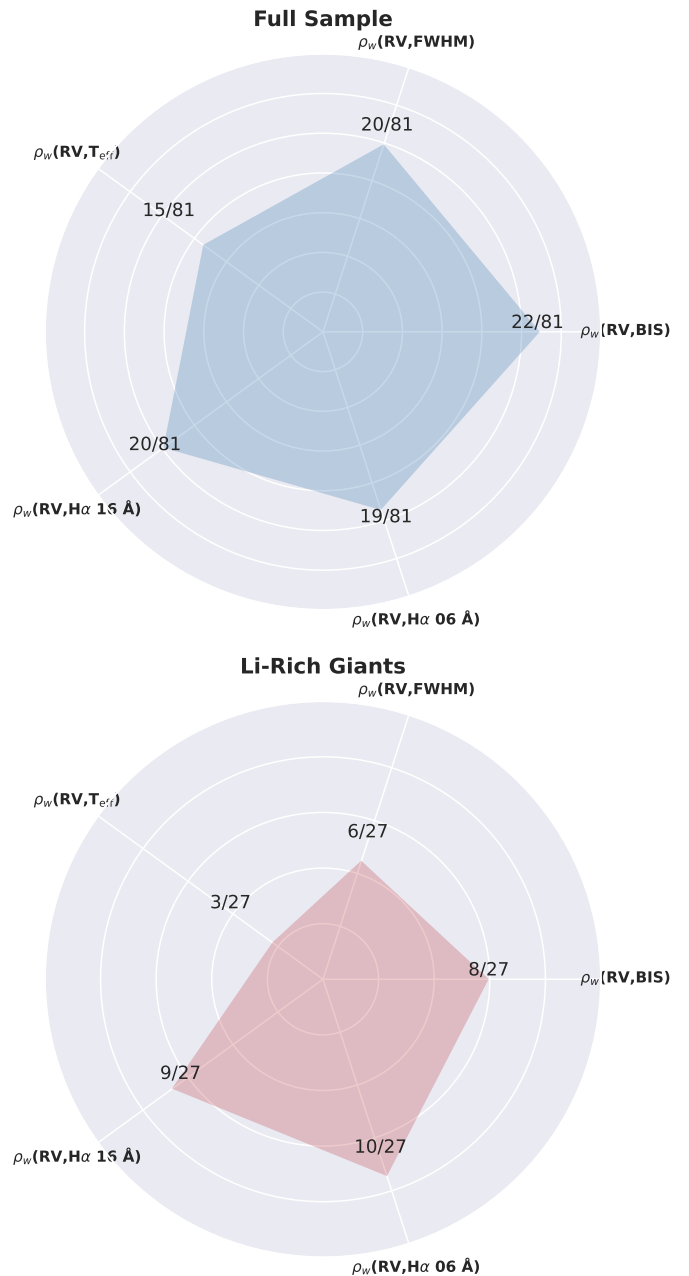


Fig. 2: Spider charts showing the amount of strong correlations found. The top chart shows the amount of strong correlations found between RV and every stellar activity indicator in the full sample of red giant stars. The bottom chart shows the amount of strong correlations found between RV and every stellar activity indicator for the stars of interest listed in Table 2.

Overall, correlations were found for stars in various evolutionary stages and of different mass ranges as well. This is evidenced in the Hertzsprung–Russell (HR) diagram Figure 3, where different symbols indicate different numbers of strong correlations found per star, and the data points are sized according to stellar mass. In general, all symbols display a range of sizes and are distributed across the HR diagram revealing there is no preferred mass or age for correlations to be found. A summary of the significant correlations discussed can be found in Tables 4 and 5. Something to note from Table 5 is that inhabitants of cluster NGC6705, in general, show higher amounts of Li than

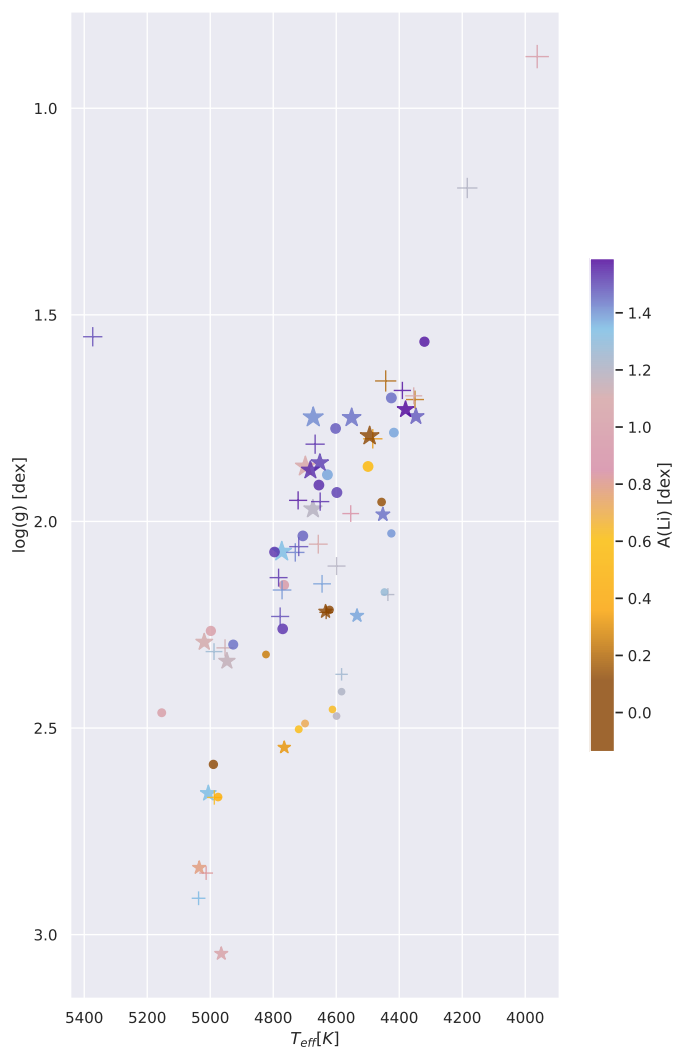


Fig. 3: HR diagram of all the stars in our sample. Here we use the $\log(g)$ and T_{eff} derived in Tsantaki et al. (2023) for each star. The stars are colored according to $A(\text{Li})$, and have different sizes to represent different masses. The different symbols are an indicative of how many strong correlations were found in a particular star: "•" indicates 0 strong correlations, "★" indicates 1 strong correlation and "+" indicates 2 or more strong correlations.

the rest of the stars in our sample. These stars are particular as they also demonstrate unusually high amounts of α -elements for their young age (e.g. Casamiquela et al. 2018). Messina et al. (2010) found that the G type stars of this cluster retain higher levels of activity up to the age of the cluster. We find that, 19/28 of these stars show at least one significant correlation with one of the parameters at study and 22/28 are fast rotators (see Table 5). So in general, the stars in this cluster are magnetically active and also rotate fast which could be connected to the abnormally high levels of Li observed.

In Figure 4 we show a violin plot of $A(\text{Li})$ as a function of the number of strong correlations observed per star. We may see that the density of points increases towards higher values of $A(\text{Li})$ with increasing number of correlations found. This is evidenced by the increasing width of the violins from left to right in high $A(\text{Li})$ regions and by the central tendency being slightly higher for stars that show 1 or more than 2 correlations between RV and stellar activity indicators. As such, strong correlations tend

to appear more often for stars with higher amounts of Li in their atmospheres. Such a result also indicates that $A(\text{Li})$ seems to be connected with higher levels of stellar activity in our sample.

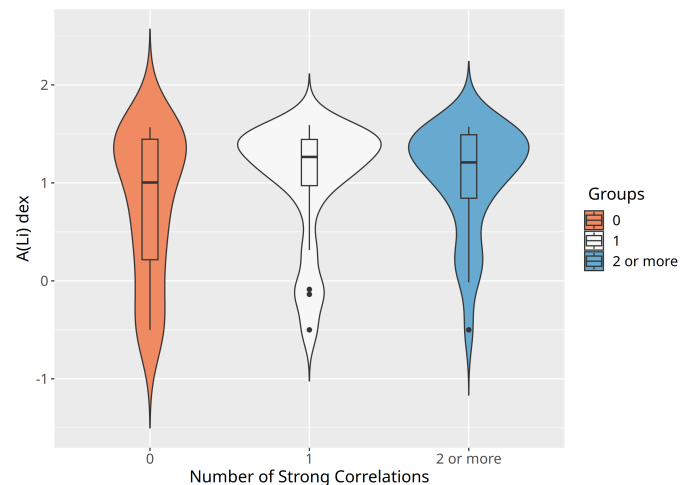


Fig. 4: Violin plot of $A(\text{Li})$ as a function of the number of strong correlations observed per star. From left to right each violin represents the distribution of the number of strong correlations found (0, 1 or ≥ 2) relatively to $A(\text{Li})$. Inside each violin is a box delimiting the interquartile range. The thick black line appearing inside each box is the median of the distribution. Each box also has a lower and upper whisker that span from minimum to maximum $A(\text{Li})$ in each distribution. Points seen beyond the whiskers are outliers.

To complement the correlation analysis, GLSP of RV and stellar activity indicators were also plotted for all stars. GLSP are often used when analysing whether variability observed in RV signals is caused by the existence of a companion or by stellar activity. This is because, they allow us to determine if there is periodic variability occurring at the stellar surface that is equivalent to periodic variability observed in RV. It has been shown that magnetic phenomena appearing at the stellar surface can introduce variability in RV that is at a different phase relatively to variability observed in stellar activity indicator signals (e.g. Queloz et al. 2001; Santos et al. 2014; Delgado Mena et al. 2018). As such, when looking for correlations between RV and activity proxies we may obtain a weak correlation coefficient, but this does not necessarily mean that RV variability does not originate from stellar activity. Thus, finding peaks at similar periods in RV and again in different stellar activity signals with GLSP, is also an indicator that RV variability connects with stellar activity.

The results of the GLSP analysis are also presented in Tables 4 and 5. In summary, stars NGC2345No50, NGC2423No3, NGC3532No670, NGC4349No127 and NGC6705No1101 show significant peaks (above a false alarm probability (FAP) level of 1%) in their RV GLSPs which consistently appear around the same period for at least one of their stellar activity indicators. All relevant GLSPs are in Appendix D and Delgado Mena et al. (2023). All of these stars can be considered Li-rich (see Table 2) and most of them also present long-term and large amplitude RV variations which mimic the presence of planets but are of probable stellar origin (Delgado Mena et al. 2023). These stars with periodic RV variations lie on the RGB or RGB tip (they are among the most luminous in their cluster) rather than in

the red clump, as found in recent works for super-Li-rich stars (Singh et al. 2019; Kumar et al. 2020). Interestingly, Jorissen et al. (2020) studying the binarity fraction of Li-rich giants found that some of the most luminous Li-rich giants show RV variability not caused by stellar companions, though no information about stellar activity is provided by the authors. In a similar way, Gonçalves et al. (2020) finds hints of RV variability in several Li-rich stars with detected longitudinal magnetic field, but the quantity of data does not allow to discern the real origin of such variability.

5. Conclusions

In summary based on the results from HARPS data, we find that the variability of BIS and FWHM and the mean and median of $H\alpha$ increase exponentially with $A(\text{Li})$. This leads us to conclude that the stars in our sample that are more magnetically active also show higher amounts of Li in their atmosphere. We also find that stars with higher amounts of Li tend to show more correlations between RV and stellar activity indicators. The majority of stars, 19/27 (10/14 leaving aside the special cluster NGC6705), that can be considered Li-rich in this work, either show correlations of RV with at least one of the stellar activity indicators or show periodic variability in at least one of the stellar activity indicator signals with a similar period in RV. From the GLSP analysis we may also conclude that almost all the stars with strong RV variations that mimic the presence of planets are Li-rich (see also, Delgado Mena et al. 2016). This is particularly important when searching for exoplanets orbiting evolved stars, since our results show that detecting periodic RV variability in red giants with high $A(\text{Li})$ might be a signature of stellar activity instead of planets. It is interesting to note that Adamów et al. (2018) reported a higher than expected fraction of planetary companions around the Li-rich stars in their sample, pointing to a connection between Li enrichment and planetary presence/engulfment. However, the orbits they find are quite eccentric, something not expected if the RV were of stellar origin, and that supports the hypothesis of inner planets engulfment. The Li-rich stars with strong RV variability discussed here lie on the RGB or RGB tip, however, stars showing correlations between Li abundance and activity level are found all across the HR diagram. This might indicate that mild Li enrichment (since we do not have super-Li-rich giants in our sample) connected to stellar activity can occur at different evolutionary stages, but a large enhancement of Li is more particular and can only occur at certain evolutionary stages, such as, the He-flash (Singh et al. 2019; Kumar et al. 2020). It is still not clear then, whether the strong RV variability of mild Li-rich giants on the RGB is connected to their evolutionary stage and the possible super-Li rich phase to happen soon after (at the beginning of the He-core burning phase), or if it is a consequence of stellar activity.

Acknowledgements. I.R. and E.D.M. acknowledge the support from Fundação para a Ciência e a Tecnologia (FCT) through national funds and from FEDER through COMPETE2020 by the following grants: UIDB/04434/2020 & UIDP/04434/2020. I.R. acknowledges the support from FCT through the grant 2022.03993.PTDC. E.D.M. acknowledges the support from FCT through Stimulus FCT contract 2021.01294.CEECIND. E.D.M and J.G.S. acknowledge the support from FCT through the grant 2022.04416.PTDC.

References

Adamów, M., Niedzielski, A., Kowalik, K., et al. 2018, *A&A*, 613, A47
 Adamów, M., Niedzielski, A., Villaver, E., Nowak, G., & Wolszczan, A. 2012, *ApJ*, 754, L15

Adamów, M., Niedzielski, A., Villaver, E., Wolszczan, A., & Nowak, G. 2014, *A&A*, 569, A55
 Aguilera-Gómez, C., Chanamé, J., Pinsonneault, M. H., & Carlberg, J. K. 2016, *ApJ*, 829, 127
 Aguilera-Gómez, C., Jones, M. I., & Chanamé, J. 2023, *A&A*, 670, A73
 Bagdonas, V., Drazdauskas, A., Tautvaišienė, G., Smiljanic, R., & Chorniy, Y. 2018, *Astronomy and Astrophysics*, 615, A165
 Brown, J. A., Sneden, C., Lambert, D. L., & Dutchover, Edward, J. 1989, *ApJS*, 71, 293
 Cameron, A. G. W. & Fowler, W. A. 1971, *ApJ*, 164, 111
 Cantiello, M. & Langer, N. 2010, *A&A*, 521, A9
 Carlberg, J. K., Cunha, K., Smith, V. V., & Majewski, S. R. 2012, *ApJ*, 757, 109
 Casamiquela, L., Carrera, R., Balaguer-Núñez, L., et al. 2018, *A&A*, 610, A66
 Casey, A. R., Ruchti, G., Masseron, T., et al. 2016, *MNRAS*, 461, 3336
 Charbonnel, C. 1994, *A&A*, 282, 811
 Charbonnel, C. 1995, *ApJ*, 453, L41
 Charbonnel, C. & Balachandran, S. C. 2000, arXiv preprint astro-ph/0005280
 de Medeiros, J. R., Melo, C. H. F., & Mayor, M. 1996, *A&A*, 309, 465
 Deepak & Reddy, B. E. 2019, *MNRAS*, 484, 2000
 Delgado Mena, E., Gomes da Silva, J., Faria, J. P., et al. 2023, *A&A*, 679, A94
 Delgado Mena, E., Lovis, C., Santos, N. C., et al. 2018, *A&A*, 619, A2
 Delgado Mena, E., Tsantaki, M., Sousa, S., et al. 2016, *Astronomy & Astrophysics*, 587, A66
 Denissenkov, P. A. & Herwig, F. 2004, *ApJ*, 612, 1081
 Eggleton, P. P., Dearborn, D. S. P., & Lattanzio, J. C. 2008, *ApJ*, 677, 581
 Favata, F., Micela, G., & Sciortino, S. 1996, *A&A*, 311, 951
 Fekel, F. C. & Balachandran, S. 1994, in *Cool Stars, Stellar Systems, and the Sun*, Vol. 64, 279
 Frinchaboy, P. M. & Majewski, S. R. 2008, *The Astronomical Journal*, 136, 118
 Gao, Q., Shi, J.-R., Yan, H.-L., et al. 2019, *ApJS*, 245, 33
 Gomes da Silva, J., Bensabat, A., Monteiro, T., & Santos, N. C. 2022, *A&A*, 668, A174
 Gomes da Silva, J., Figueira, P., Santos, N., & Faria, J. 2018, *Journal of Open Source Software*, 3, 667
 Gomes da Silva, J., Santos, N. C., Adibekyan, V., et al. 2021, *A&A*, 646, A77
 Gonçalves, B. F. O., da Costa, J. S., de Almeida, L., Castro, M., & do Nascimento, J. D., J. 2020, *MNRAS*, 498, 2295
 Herzog, A. D., Sanders, W. L., & Seggewiss, W. 1975, *Astronomy and Astrophysics Supplement Series*, 19, 211
 Holanda, N., Pereira, C. B., & Drake, N. A. 2019, *MNRAS*, 482, 5275
 Holanda, N., Ramos, A. A., Peña Suárez, V. J., Martínez, C. F., & Pereira, C. B. 2022, *Monthly Notices of the Royal Astronomical Society*, 516, 4484
 Iben, Icko, J. 1967a, *ApJ*, 147, 650
 Iben, Icko, J. 1967b, *ApJ*, 147, 624
 Jorissen, A., Van Winckel, H., Siess, L., et al. 2020, *A&A*, 639, A7
 Katime Santrich, O. J., Pereira, C. B., & Drake, N. A. 2013, *Astronomy and Astrophysics*, 554, A2
 Kirby, E. N., Guhathakurta, P., Zhang, A. J., et al. 2016, 819, 135
 Kowkabany, J., Ezzeddine, R., Charbonnel, C., et al. 2022, arXiv e-prints, arXiv:2209.02184
 Kumar, Y. B., Reddy, B. E., Campbell, S. W., et al. 2020, *Nature Astronomy*, 4, 1059
 Kumar, Y. B., Reddy, B. E., & Lambert, D. L. 2011, *ApJ*, 730, L12
 Lagarde, N., Minkevičiūtė, R., Drazdauskas, A., et al. 2024, *A&A*, 684, A70
 Liu, Y. J., Tan, K. F., Wang, L., et al. 2014, *ApJ*, 785, 94
 Lovis, C. & Mayor, M. 2007, *Astronomy and Astrophysics*, 472, 657
 Luck, R. E. 1994, *The Astrophysical Journal Supplement Series*, 91, 309
 Lyubimkov, L. S. 2016, *Astrophysics*, 59, 411
 Martell, S. L., Simpson, J. D., Balasubramanian, A. G., et al. 2021, *MNRAS*, 505, 5340
 Mayor, M., Pepe, F., Queloz, D., et al. 2003, *The Messenger*, 114, 20
 Mermilliod, J. C., Mayor, M., & Udry, S. 2008, *Astronomy and Astrophysics*, 485, 303
 Messina, S., Parihar, P., Koo, J.-R., et al. 2010, *A&A*, 513, A29
 Pabst, C. H. M., Goicoechea, J. R., Teyssier, D., et al. 2020, *A&A*, 639, A2
 Palacios, A., Charbonnel, C., Talon, S., & Siess, L. 2004, arXiv e-prints, astro-ph/0403185
 Pallavicini, R., Randich, S., & Giampapa, M. 1992, *Astronomy and Astrophysics*, 253, 185
 Patton, R. A., Pinsonneault, M. H., Cao, L., et al. 2023, arXiv e-prints, arXiv:2303.08151
 Peña Suárez, V. J., Sales Silva, J. V., Katime Santrich, O. J., Drake, N. A., & Pereira, C. B. 2018, *ApJ*, 854, 184
 Queloz, D., Henry, G. W., Sivan, J. P., et al. 2001, *A&A*, 379, 279
 Queloz, D., Mayor, M., Weber, L., et al. 2000, *Astronomy and Astrophysics*, 354, 99
 Randich, S., Pasquini, L., Franciosini, E., et al. 2020, *A & A*, 640, L1
 Romano, D., Magrini, L., Randich, S., et al. 2021, *A & A*, 653, A72
 Santos, N. C., Mortier, A., Faria, J. P., et al. 2014, *A&A*, 566, A35
 Santos, N. C., Udry, S., Mayor, M., et al. 2003, *A&A*, 406, 373

- Sayeed, M., Ness, M. K., Montet, B. T., et al. 2023, arXiv e-prints, arXiv:2306.03323
- Singh, R., Reddy, B. E., Bharat Kumar, Y., & Antia, H. M. 2019, ApJ, 878, L21
- Smiljanic, R., Gauderon, R., North, P., et al. 2009, A&A, 502, 267
- Snedden, C., Afşar, M., Bozkurt, Z., et al. 2022, ApJ, 940, 12
- Snedden, C. A. 1973, PhD thesis, University of Texas
- Sun, Q., Deliyannis, C. P., Twarog, B. A., et al. 2022, Monthly Notices of the Royal Astronomical Society, 513, 5387
- Tayar, J., Ceillier, T., García-Hernández, D. A., et al. 2015, ApJ, 807, 82
- Tsantaki, M., Andreasen, D. T., Teixeira, G. D. C., et al. 2018, MNRAS, 473, 5066
- Tsantaki, M., Delgado-Mena, E., Bossini, D., et al. 2023, A&A, 674, A157
- Udry, S., Mayor, M., Naef, D., et al. 2000, Astronomy and Astrophysics, 356, 590
- Xing, L.-F., Li, Y.-C., Chang, L., Wang, C.-J., & Bai, J.-M. 2021, A&A, 653, A28
- Yana Galarza, J., Meléndez, J., Lorenzo-Oliveira, D., et al. 2019, MNRAS, 490, L86
- Zboril, M., Byrne, P. B., & Rolleston, W. R. J. R. 1997, Monthly Notices of the Royal Astronomical Society, 284, 685
- Zechmeister, M. & Kürster, M. 2009, A&A, 496, 577

Star	$\rho_w(\text{RV}, \text{BIS})$	$\rho_w(\text{RV}, \text{FWHM})$	$\rho_w(\text{RV}, T_{\text{eff}})$	$\rho_w(\text{RV}, \text{H}\alpha 1.6\text{\AA})$	$\rho_w(\text{RV}, \text{H}\alpha 0.6\text{\AA})$	A(Li) [dex]	Mass (M_{\odot})	$v \sin(i)$ (km/s)	n
IC4651No10393						-0.500	1.801	1.870	23
IC4651No11453						-0.007	2.699	1.750	33
IC4651No12935				×		0.315	1.800	0.000	5
IC4651No14527						-0.500	1.867	1.810	31
IC4651No6333	×			×		1.209	1.779	2.130	5
IC4651No7646						-0.500	2.438	0.000	31
IC4651No8540						0.715	1.797	0.000	27
IC4651No9025						0.621	1.815	0.000	30
IC4651No9122						-0.500	1.795	0.680	74
IC4651No9791						1.277	1.750	1.850	33
IC4756No14		×	×			-0.016	1.973	2.030	5
IC4756No38	×					0.783	2.005	0.000	7
IC4756No44	×				×	0.823	2.016	2.830	6
IC4756No52				×		1.447	2.272	2.870	16
NGC2345No50		×		×★	×★	0.977	5.843	5.270	26
NGC2423No3	×★	★				1.377	2.035	2.190	60
NGC2423No56				×		1.035	1.991	0.000	7
NGC3114No150	×					1.340	4.490	16.190	11
NGC3114No170	×	×		×	×	1.503	3.981	11.320	6
NGC3114No181		×	×			0.309	4.022	3.950	11
NGC3114No223			×			-0.500	2.508	0.330	8
NGC3114No238						0.533	3.807	4.090	10
NGC3114No262	×					1.190	3.884	9.220	31
NGC3114No283	×					1.415	4.663	12.470	30
NGC3114No6		×				1.092	4.612	7.480	44
NGC3532No100						0.952	3.379	4.870	19
NGC3532No122	×					1.344	2.873	9.570	20
NGC3532No160	×	×	×	×		1.125	3.149	4.780	8
NGC3532No19						1.443	3.218	5.050	46
NGC3532No221	×		×	×		0.186	4.818	5.890	22
NGC3532No522	×	×	×			1.202	4.412	12.480	6
NGC3532No596				×		1.153	3.126	7.210	31
NGC3532No670		★		★	×	1.475	3.047	4.640	29
NGC3680No13	×		×	×		1.252	1.659	0.280	7
NGC3680No26						1.192	1.704	0.960	18
NGC3680No34						0.246	1.752	3.010	12
NGC3680No41						0.633	1.641	0.000	18
NGC3680No44		×		×	×	-0.500	1.690	2.550	6
NGC3680No53						1.211	1.652	0.120	18
NGC4349No127		★				1.375	3.007	4.810	56
NGC4349No168						1.000	3.358	5.510	35
NGC4349No174		×	×			0.843	3.003	3.190	22
NGC4349No203		×				1.105	3.296	5.310	10
NGC4349No5						-0.500	3.134	7.270	35
NGC4349No9	×				×	1.262	3.005	9.580	24
NGC5822No102	×	×		×	×	1.348	2.020	5.830	5
NGC5822No1						0.126	2.274	3.120	8
NGC5822No201						1.009	2.422	1.600	23
NGC5822No240						1.401	2.071	2.830	7
NGC5822No316	×		×	×	×	0.636	2.205	0.000	7
NGC5822No375						-0.076	2.142	2.190	19
NGC5822No443		×				-0.138	2.111	1.830	8
NGC5822No8						0.431	2.262	0.360	36

Table 4: Summary of strong correlations found for the stars analyzed in clusters IC4651, IC4756, NGC2345, NGC2423, NGC3114, NGC3532, NGC3680, NGC4349 and NGC5822. Each cross represents a correlation with BIS, FWHM, T_{eff} or $\text{H}\alpha > 0.4$. Highlighted in blue are every star in this part of the sample that can be considered Li-rich, and highlighted in purple are all stars with considerable rotation, that is, $v \sin(i) > 5$ km/s. ★ indicates that a significant peak was found for the GLSP of the respective quantity which also appeared in RV. Also in this table are the values of the mass for each star (M) as well as the number of points (n) used to calculate the correlations.

Star	$\rho_w(\text{RV,BIS})$	$\rho_w(\text{RV,FWHM})$	$\rho_w(\text{RV,T}_{\text{eff}})$	$\rho_w(\text{RV,H}\alpha 1.6\text{\AA})$	$\rho_w(\text{RV,H}\alpha 0.6\text{\AA})$	A(Li) [dex]	Mass (M_{\odot})	$v \sin(i)$ (km/s)	n
NGC6705No1090						1.380	3.800	6.050	9
NGC6705No1101	★					1.527	3.674	11.240	25
NGC6705No1111		×		×		1.425	3.618	7.110	10
NGC6705No1117				×	×	1.567	3.521	9.440	10
NGC6705No1145	×	×				1.385	3.355	7.300	11
NGC6705No1184			×	×		0.215	3.448	4.420	11
NGC6705No1248		×		×		1.525	3.455	8.430	9
NGC6705No1256	×					1.591	3.146	4.470	14
NGC6705No1286	×				×	1.400	3.709	9.940	21
NGC6705No1364						1.530	3.670	12.240	13
NGC6705No136			×		×	1.082	3.792	3.730	7
NGC6705No1423						1.455	3.852	5.480	13
NGC6705No1446			×	×	×	1.194	3.451	7.140	6
NGC6705No160						1.477	3.740	6.950	22
NGC6705No1625	×				×	1.088	3.087	4.100	19
NGC6705No1658						1.512	3.910	7.290	28
NGC6705No1837	×	×	×			1.495	3.493	10.520	9
NGC6705No2000					×	1.443	4.040	4.760	12
NGC6705No320		×		×	×	1.492	3.876	5.500	8
NGC6705No411		×		×	×	1.573	3.193	6.470	8
NGC6705No660		×	×		×	1.533	3.577	5.740	7
NGC6705No669					×	1.511	3.451	8.930	6
NGC6705No686						1.467	3.727	9.480	6
NGC6705No779						1.569	3.397	5.570	22
NGC6705No816			×		×	1.533	3.956	8.770	6
NGC6705No827		×				-0.087	4.040	4.800	8
NGC6705No916	×					1.532	3.745	9.700	9
NGC6705No963						1.542	3.757	6.710	9

Table 5: Summary of strong correlations found for the stars analyzed in cluster NGC6705. Each cross represents a correlation with BIS, FWHM, T_{eff} or $\text{H}\alpha > 0.4$. Highlighted in blue are every star in this part of the sample that can be considered Li-rich, and highlighted in purple are all stars with considerable rotation, that is, $v \sin(i) > 5$ km/s. ★ indicates that a significant peak was found for the GLSP of the respective quantity which also appeared in RV. Also in this table are the values of the mass for each star (M) as well as the number of points (n) used to calculate the correlations.

Appendix A: Methods for Data Analysis

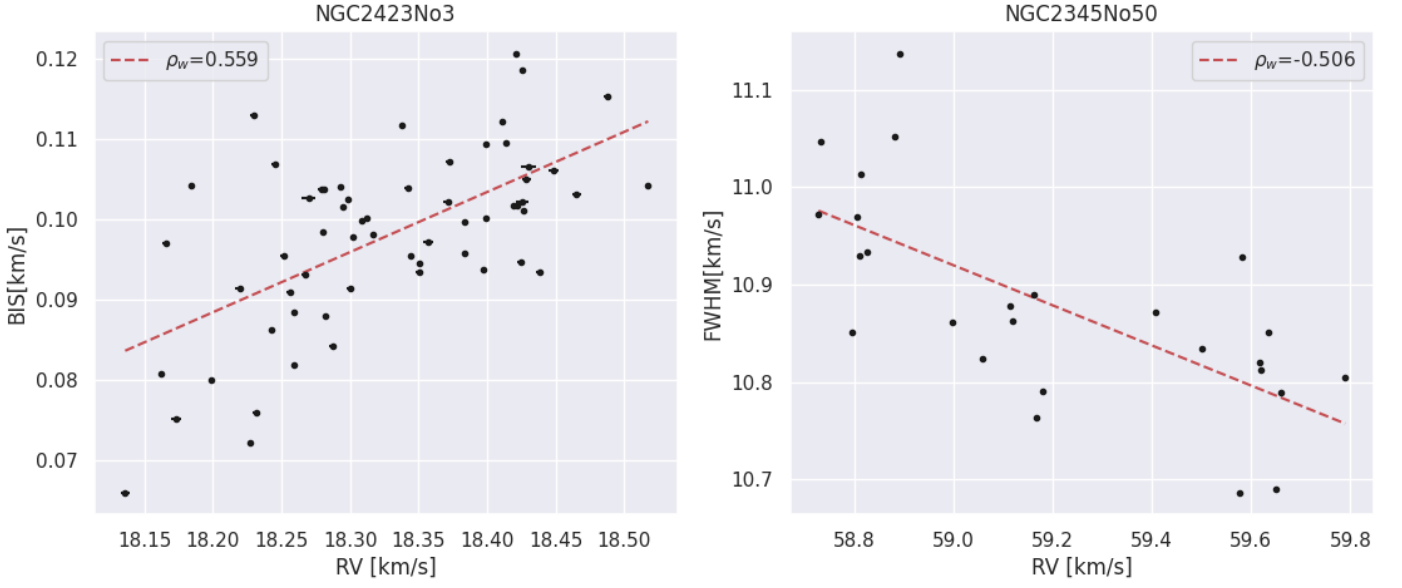


Fig. A.1: Example of strong correlations found for stars NGC2423No3 (left) and NGC2345No50 (right). NGC2423No3 shows a strong positive correlation between RV and BIS, while NGC2345No50 shows a strong negative correlation between RV and FWHM.

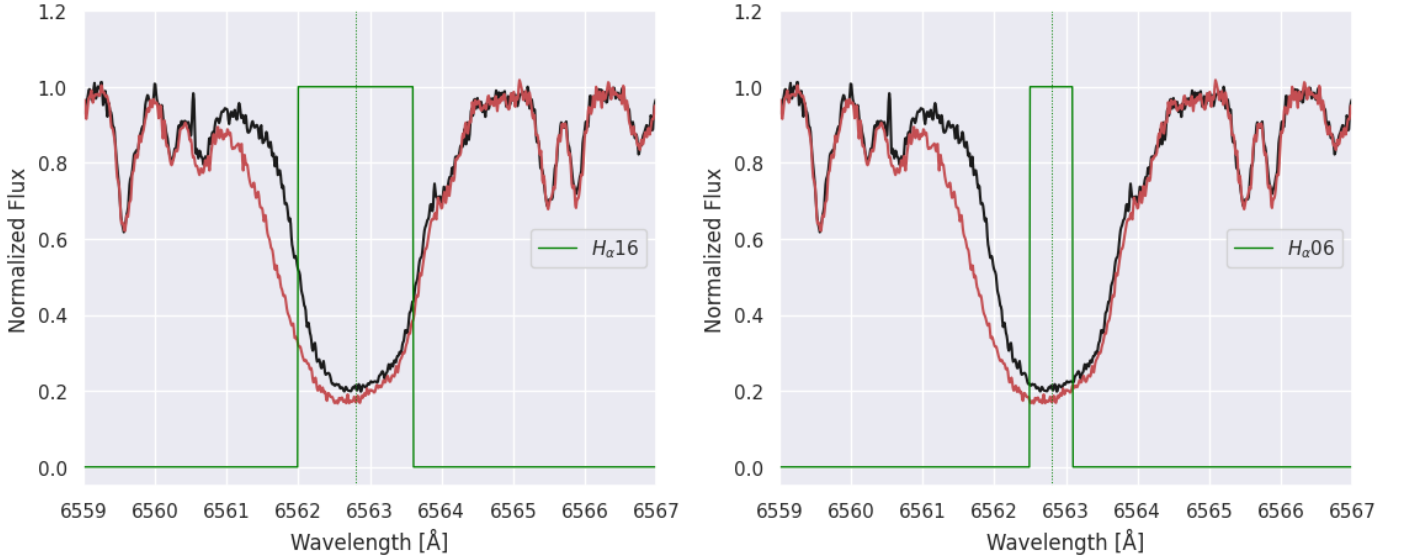


Fig. A.2: Example of the $H\alpha$ line profile difference of two spectra obtained at different times for star NGC2345No50 (depicted by the black and red lines). In green are represented the two different bandpasses ($H\alpha16$ on the left and $H\alpha06$ on the right), around the $H\alpha$ line center, used to compute the $H\alpha$ index for the individual spectra of the stars with ACTIN 2.

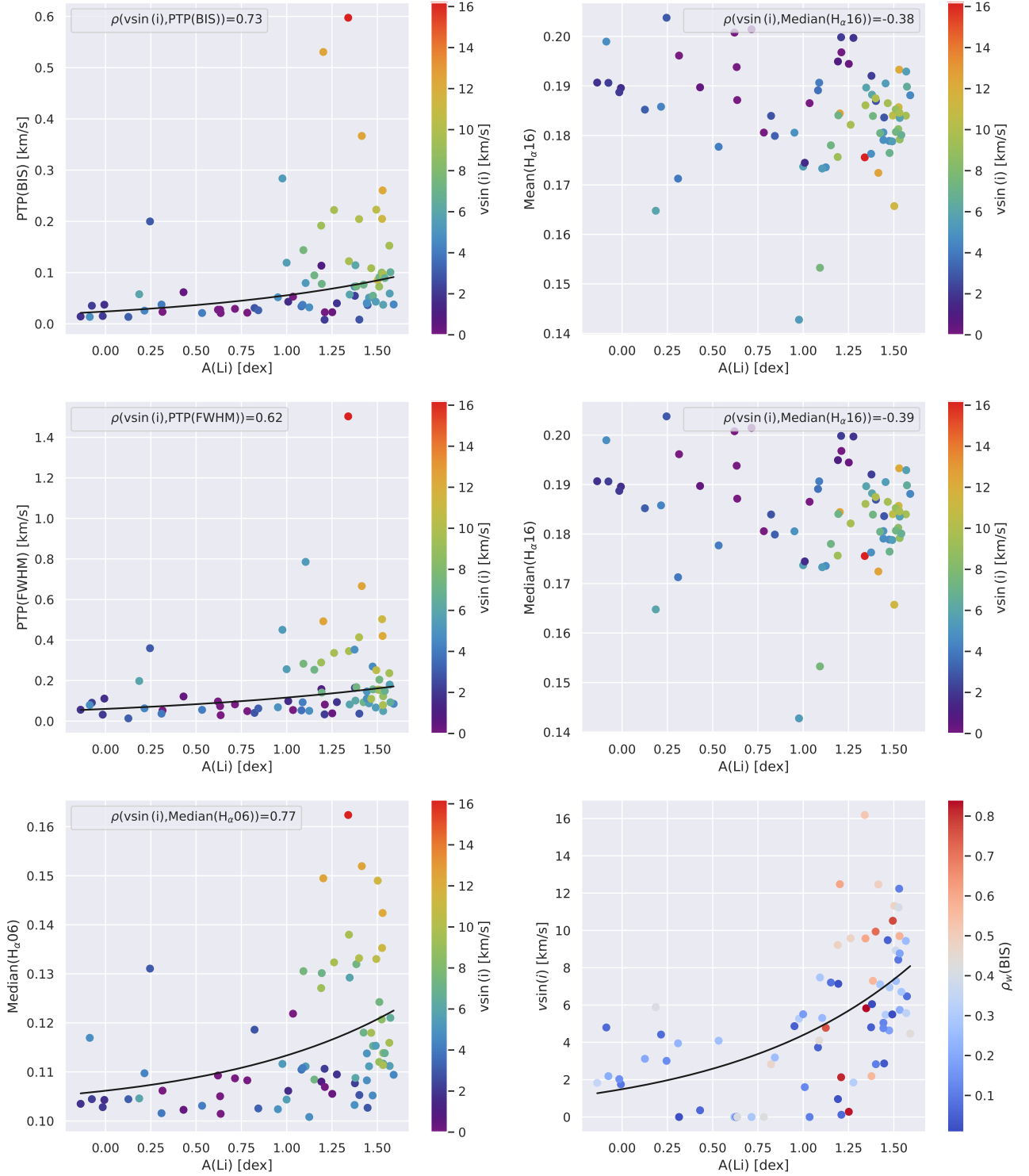
Appendix B: Statistically Significant Relations


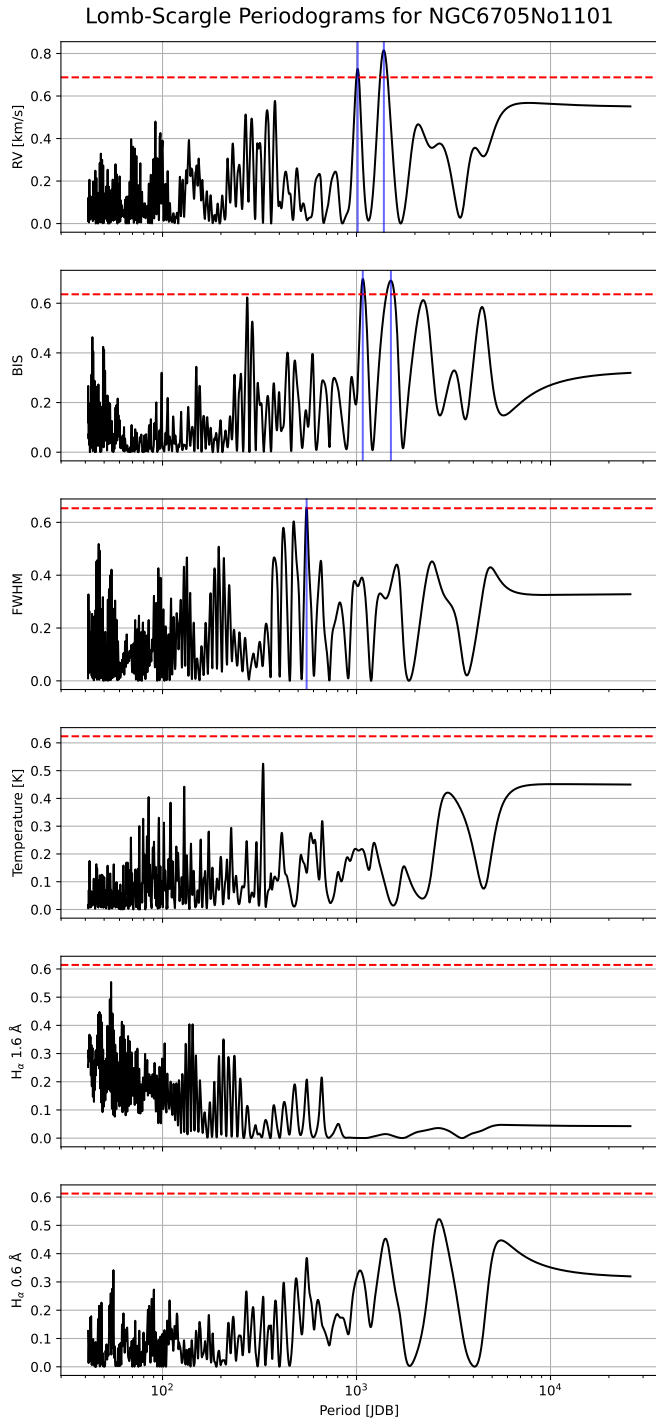
Fig. B.1: **Left:** Exponential relation found between the PTP of BIS data for each star and A(Li) [top panel]; the PTP of FWHM data for each star and A(Li) [middle panel]; the median of $H\alpha 06$ data for each star and A(Li) [bottom panel]. The data points are colored according to the $v \sin(i)$ of each star. The black line is the line of best fit. In these plots we also show the Pearson Correlation Coefficients (ρ) between the activity proxies used and $v \sin(i)$, all of them being very strong (> 0.6). **Right:** No relation found between the mean and median of $H\alpha 16$ data for each star and A(Li) [top and middle panels, respectively]. Here again the data points are colored according to the $v \sin(i)$ of each star and ρ between the activity proxies and $v \sin(i)$ is also shown, being weak in both cases. In the bottom panel we show the exponential relation found between $v \sin(i)$ and A(Li). The data points are colored according to the strength of the correlations of $\rho_w(\text{BIS})$ to demonstrate that the majority of correlations found for this indicator appear for moderate and fast rotators ($v \sin(i) > 5$ km/s). The black line is the line of best fit.

Appendix C: Correlation Tables

Star	ρ_{ν} (RV,BIS)	p(BIS)	ρ_{ν} (RV,FWHM)	p(FWHM)	ρ_{ν} (RV,T _{eff})	p(T _{eff})	ρ_{ν} (RV,H α 1.6Å)	p(H α 1.6Å)	ρ_{ν} (RV,H α 0.6Å)	p(H α 0.6Å)	A(Li) [dex]	Mass (M _⊙)	v sin(i) (km/s)	n	
IC4651No10393	-0.12	0.58	-0.03	0.89	-0.11	0.63	-0.25	0.26	-0.32	0.14	-0.500	1.801	1.870	23	
IC4651No11453	-0.09	0.62	0.06	0.75	0.17	0.33	0.01	0.95	-0.001	0.996	-0.007	2.699	1.750	33	
IC4651No12935	-0.02	0.98	0.25	0.68	0.11	0.86	-0.44	0.45	0.07	0.91	0.315	1.800	0.000	5	
IC4651No14527	-0.02	0.90	0.03	0.88	0.23	0.22	-0.29	0.12	-0.34	0.06	-0.500	1.867	1.810	31	
IC4651No6333	-0.81	0.10	0.28	0.64	-0.13	0.84	-0.65	0.23	-0.23	0.71	1.209	1.779	2.130	5	
IC4651No7646	-0.01	0.95	0.29	0.13	0.02	0.90	-0.13	0.49	-0.18	0.34	-0.500	2.438	0.000	31	
IC4651No8540	-0.28	0.15	0.24	0.23	-0.01	0.97	-0.24	0.24	0.23	0.25	0.715	1.797	0.000	27	
IC4651No9025	-0.23	0.24	0.09	0.66	-0.12	0.55	0.20	0.33	-0.22	0.26	0.621	1.815	0.000	30	
IC4651No9122	0.18	0.13	-0.12	0.33	-0.05	0.66	0.10	0.41	0.19	0.11	-0.500	1.795	0.680	74	
IC4651No9791	-0.32	0.07	0.03	0.85	-0.07	0.70	0.07	0.69	0.07	0.71	1.277	1.750	1.850	33	
IC4756No14	-0.14	0.82	0.69	0.19	-0.65	0.24	0.06	0.92	0.25	0.68	-0.016	1.973	2.030	5	
IC4756No38	-0.42	0.26	-0.10	0.79	0.01	0.98	-0.29	0.45	0.31	0.42	0.783	2.005	0.000	7	
IC4756No44	0.46	0.35	0.06	0.90	-0.16	0.77	-0.23	0.67	0.51	0.30	0.823	2.016	2.830	6	
IC4756No52	0.04	0.90	-0.08	0.78	-0.26	0.35	0.92	1.54E-06	-0.08	0.77	1.447	2.272	2.870	16	
NGC2345No50	0.31	0.12	-0.51	0.01	0.02	0.91	0.60	1.07E-03	0.56	2.86E-03	0.977	5.843	5.270	26	
NGC2423No3	0.56	3.40E-06	0.28	0.03	0.11	0.40	0.03	0.79	-0.07	0.61	1.377	2.035	2.190	60	
NGC2423No56	-0.11	0.82	0.12	0.79	-0.07	0.88	-0.91	4.38E-03	0.04	0.93	1.035	1.991	0.000	7	
NGC3114No150	-0.52	0.10	-0.06	0.86	0.19	0.58	-0.17	0.61	-0.24	0.47	1.340	4.490	16.190	11	
NGC3114No170	-0.48	0.34	-0.54	0.27	0.25	0.64	-0.62	0.19	-0.62	0.19	1.503	3.981	11.320	6	
NGC3114No181	-0.23	0.47	0.62	0.03	-0.59	0.04	0.40	0.20	0.26	0.42	0.309	4.022	3.950	11	
NGC3114No223	-0.19	0.64	-0.23	0.59	-0.49	0.22	0.17	0.69	0.07	0.87	-0.500	2.508	0.330	8	
NGC3114No238	0.26	0.44	0.26	0.44	-0.01	0.97	0.29	0.38	0.15	0.65	0.533	3.807	4.090	10	
NGC3114No262	-0.48	0.01	-0.03	0.89	0.29	0.11	-0.04	0.82	0.16	0.39	1.190	3.884	9.220	31	
NGC3114No283	0.49	0.01	0.20	0.30	0.09	0.64	0.06	0.74	0.27	0.15	1.415	4.663	12.470	30	
NGC3114No6	-0.28	0.06	-0.42	4.81E-03	-0.18	0.23	0.35	0.02	0.32	0.03	1.092	4.612	7.480	44	
NGC3532No100	0.05	0.85	0.20	0.41	-0.14	0.56	0.19	0.43	0.09	0.71	0.952	3.379	4.870	19	
NGC3532No122	-0.60	4.94E-03	0.14	0.56	0.09	0.70	0.08	0.74	0.14	0.54	1.344	2.873	9.570	20	
NGC3532No160	-0.75	0.03	0.53	0.18	-0.65	0.08	0.56	0.15	0.19	0.65	1.125	3.149	4.780	8	
NGC3532No19	-0.12	0.44	-0.07	0.66	0.11	0.47	0.20	0.17	-0.11	0.45	1.443	3.218	5.050	46	
NGC3532No221	-0.41	0.05	-0.27	0.20	0.62	1.58E-03	-0.41	0.05	0.10	0.66	0.186	4.818	5.890	22	
NGC3532No522	-0.61	0.20	0.79	0.06	0.43	0.39	0.02	0.97	0.10	0.85	1.202	4.412	12.480	6	
NGC3532No596	0.08	0.66	0.01	0.95	0.13	0.49	-0.60	3.15E-04	0.10	0.61	1.153	3.126	7.210	31	
NGC3532No649	-0.26	0.08	0.10	0.49	0.06	0.69	0.13	0.36	0.16	0.26	3.271	2.167	0.000	49	
NGC3532No670	0.18	0.34	-0.13	0.49	0.09	0.63	0.35	0.06	0.42	0.02	1.475	3.047	4.640	29	
NGC3680No13	0.83	0.02	0.08	0.86	0.58	0.18	0.45	0.31	0.39	0.38	1.252	1.659	0.280	7	
NGC3680No26	0.02	0.94	0.06	0.82	0.17	0.50	0.28	0.27	0.35	0.15	1.192	1.704	0.960	18	
NGC3680No34	-0.13	0.68	-0.38	0.22	0.02	0.95	-0.12	0.71	-0.15	0.22	0.64	0.246	1.752	3.010	12
NGC3680No41	-0.03	0.91	-0.15	0.55	0.20	0.42	0.16	0.53	0.01	0.97	0.633	1.641	0.000	18	
NGC3680No44	-0.02	0.98	0.79	0.06	0.00	0.99	0.77	0.08	0.46	0.36	-0.500	1.690	2.550	6	
NGC3680No53	-0.06	0.81	-0.04	0.88	0.31	0.20	-0.03	0.91	-0.10	0.70	1.211	1.652	0.120	18	
NGC4349No127	0.04	0.76	-0.03	0.80	-0.07	0.59	0.26	0.05	0.11	0.44	1.375	3.007	4.810	56	
NGC4349No168	-0.17	0.34	0.13	0.46	-0.04	0.81	-0.07	0.69	0.03	0.85	1.000	3.358	5.510	35	
NGC4349No174	-0.25	0.25	-0.51	0.02	0.50	0.02	0.07	0.76	0.08	0.72	0.843	3.003	3.190	22	
NGC4349No203	0.24	0.50	-0.47	0.17	0.15	0.69	0.27	0.45	0.21	0.56	1.105	3.296	5.310	10	
NGC4349No5	-0.24	0.16	-0.37	0.03	0.37	0.03	-0.04	0.84	-0.05	0.79	-0.500	3.134	7.270	35	
NGC4349No9	-0.48	0.02	0.37	0.07	-0.04	0.86	0.13	0.53	0.57	3.24E-03	1.262	3.005	9.580	24	
NGC5822No102	-0.84	0.07	1.00	1.20E-09	0.33	0.59	-0.68	0.20	-0.68	0.21	1.348	2.020	5.830	5	
NGC5822No1	-0.20	0.63	0.10	0.81	-0.05	0.91	-0.02	0.96	0.03	0.95	0.126	2.274	3.120	8	
NGC5822No201	-0.13	0.56	-0.21	0.34	-0.38	0.07	-0.12	0.58	-0.09	0.68	1.009	2.422	1.600	23	
NGC5822No240	-0.11	0.82	-0.26	0.58	-0.16	0.73	-0.20	0.67	-0.20	0.67	1.401	2.071	2.830	7	
NGC5822No316	-0.41	0.36	0.12	0.80	-0.53	0.22	0.59	0.16	0.40	0.37	0.636	2.205	0.000	7	
NGC5822No375	-0.21	0.37	-0.07	0.76	-0.35	0.13	-0.39	0.09	-0.19	0.41	-0.076	2.142	2.190	19	
NGC5822No443	-0.35	0.40	0.43	0.29	-0.31	0.46	0.26	0.54	-0.20	0.64	-0.138	2.111	1.830	8	
NGC5822No8	-0.061	0.724	0.151	0.379	-0.100	0.563	0.119	0.490	0.042	0.807	0.431	2.262	0.360	36	
NGC6705No1090	0.01	0.98	0.23	0.56	-0.08	0.84	-0.08	0.84	0.11	0.78	1.380	3.800	6.050	9	
NGC6705No1101	-0.40	0.05	0.22	0.29	0.12	0.57	-0.15	0.46	0.13	0.53	1.527	3.674	11.240	25	
NGC6705No1111	-0.28	0.43	-0.48	0.16	0.27	0.45	0.55	0.10	0.02	0.95	1.425	3.618	7.110	10	
NGC6705No1117	-0.25	0.49	-0.13	0.72	0.22	0.54	-0.57	0.09	-0.47	0.17	1.567	3.521	9.440	10	
NGC6705No1145	-0.56	0.07	0.68	0.02	0.39	0.23	-0.02	0.96	0.28	0.40	1.385	3.355	7.300	11	
NGC6705No1184	-0.07	0.84	0.14	0.69	0.43	0.19	-0.50	0.11	-0.25	0.45	0.215	3.448	4.420	11	
NGC6705No1248	0.09	0.82	0.44	0.24	0.27	0.48	-0.50	0.17	-0.29	0.45	1.525	3.455	8.430	9	
NGC6705No1256	0.43	0.12	-0.15	0.61	0.28	0.34	0.11	0.71	-0.32	0.27	1.591	3.146	4.470	14	
NGC6705No1286	-0.71	3.99E-04	-0.35	0.13	0.11	0.63	0.20	0.39	0.67	1.32E-03	1.400	3.709	9.940	21	
NGC6705No1364	-0.11	0.73	0.31	0.30	0.05	0.87	0.26	0.38	0.32	0.28	1.530	3.670	12.240	13	
NGC6705No136	0.05	0.91	0.10	0.83	0.47	0.29	-0.17	0.71	-0.44	0.32	1.082	3.792	3.730	7	
NGC6705No1423	-0.31	0.31	0.08	0.79	0.15	0.63	0.25	0.41	-0.15	0.63	1.455	3.852	5.480	13	
NGC6705No1446	-0.02	0.97	0.34	0.51	0.67	0.14	-0.58	0.23	0.83	0.04	1.194	3.451	7.140	6	
NGC6705No160	-0.29	0.19	0.29	0.19	0.22	0.33	-0.11	0.62	0.11	0.63	1.477	3.740	6.950	22	
NGC6705No1625	-0.44	0.06	-0.11	0.66	0.25	0.31	-0.20	0.40	0.41	0.08	1.088	3.087	4.100	19	
NGC6705No1658	-0.26	0.19	-0.06	0.76	0.07	0.72	-0.10	0.63	0.13	0.50	1.512	3.910	7.290	28	
NGC6705No1837	-0.77	0.01	0.52	0.15	0.61	0.08	-0.03	0.94	-0.06	0.88	1.495	3.493	10.520	9	
NGC6705No2000	-0.13	0.70	-0.05	0.88	0.30	0.35	0.29	0.36	-0.44	0.16	1.443	4.040	4.760	12	
NGC6705No320	0.01	0.98	-0.44	0.27	-0.21	0.62	0.51	0.20	0.60	0.12	1.492	3.876	5.500	8	
NGC6705No411	0.07	0.86	0.61	0.11	-0.10	0.82	-0.47	0.24	0.52	0.18	1.573	3.193	6.470	8	
NGC6705No660	-0.21	0.65	-0.62	0.14	0.47	0.29	-0.11	0.82	-0.43	0.34	1.533	3.577	5.740	7	
NGC6705No669	0.38	0.46	-0.25	0.64	0.13	0.80	0.14	0.79	0.48	0.34	1.511	3.451	8.930	6	
NGC6705No686	-0.05	0.93	0.35	0.50	0.15	0.78	-0.07	0.89	-0.36	0.48	1.467	3.727	9.480	6	
NGC6705No779	0.34	0.13	-0.32	0.15	-0.18	0.43	0.18	0.43	-0.05	0.83	1.569	3.397	5.570	22	
NGC6705No816	-0.19	0.72	0.10	0.85	0.41	0.41	-0.05	0.93	-0.58	0.23	1.533	3.956	8.770	6	
NGC6705No827	0.06	0.89	-0.54	0.22	0.23	0.62	0.24	0.61	-0.03	0.95	-0.087	4.040	4.800	8	
NGC6705No916	-0.58	0.13	-0.09	0.83	0.12	0.77	-0.07	0.86	0.21	0.62	1.532	3.745	9.700	9	
NGC6705No963	-0.28	0.47	0.27	0.48											

Appendix D: Generalized Lomb-Scargle Periodograms

The remainder of the GLPs mentioned in the text can be found in [Delgado Mena et al. \(2023\)](#).



(a) Generalized Lomb-Scargle periodograms pertaining to star *NGC6705No1101* for BIS, FWHM, T_{eff} , and $H\alpha$. The red line indicates a false alarm probability level of 1%. Significant peaks are observed in the RV and BIS GLSPs at approximately the same period. There is also a significant peak observed in FWHM not related to those observed in RV.